Cement and Concrete Research 140 (2021) 106264

Contents lists available at ScienceDirect

Cement and Concrete Research

journal homepage: www.elsevier.com/locate/cemconres

Unravelling chloride transport/microstructure relationships for blended-cement pastes with the mini-migration method

William Wilson*, Fabien Georget, Karen Scrivener

Laboratory of Construction Materials, EPFL, 1015 Lausanne, Switzerland

ARTICLE INFO

Keywords:
Blended-cement pastes
Chloride ingress
Chloride migration
Porosity
Bulk conductivity
Pore solution conductivity
Pore connectivity parameter

ABSTRACT

A chloride mini-migration method is proposed to estimate effective diffusion coefficients at the scale of the cement paste and to investigate mechanisms with complementary microstructure analyses on the same material. Blended-cement pastes with a wide range of properties were investigated in this study: systems at w/b = 0.3–0.5 including Portland cement, white Portland cement, slag-Portland cement, fly ash, glass powder, and/or limestone and calcined clay. Comparisons showed the relative and combined importance of three main parameters on the effective diffusion coefficient: the porosity, the pore connectivity parameter and the conductivity of the pore solution (low values of the latter two are generally key aspects of the high resistance of blended-cement systems against chloride ingress). Notably, a general correlation for all the investigated systems was established between the effective diffusion coefficient and the bulk conductivity (whereas no simple correlation was observed between the effective diffusion coefficient and the formation factor or the pore connectivity parameter).

1. Introduction

In the past decades, service life requirements for reinforced concrete structures exposed to chlorides have risen significatively, reaching for example 125 years for non-replaceable elements of the new Champlain Bridge in Canada [1]. Developing and testing novel durable cementitious binders is thus a challenge for cement and concrete experts. However, the resistance to chloride penetration is generally qualified/quantified with simplified indicators. A better identification of key microstructure parameters and a better understanding of the mechanisms become critical for modelling and predicting chloride ingress in emerging materials, as we cannot wait for long-term field data. This paper describes a new method in which effective chloride diffusion coefficients are estimated for cement pastes with the mini-migration setup, along with complementary microstructure analyses on the same pastes. To put the new method in context, different chloride ingress testing methods are first described below. The aim is to relate each type of test to the parameters captured by the analysis rather than to provide a comprehensive review, which already exists in literature (e.g., [2–4]).

1.1. Non-steady-state chloride diffusion/migration in concrete

A common approach to test the resistance of concrete to chloride ingress is the bulk diffusion test, as shown schematically in Fig. 1a and described in NT Build 443 [5] or ASTM C1556 [6]. This approach mimics real exposure in fully-immersed conditions and forces unidirectional penetration of chlorides, using a specimen coated with epoxy on all its surfaces except one. Chlorides penetrate into the sample by diffusion while chlorides are partly bound by the cement paste (either chemically into Friedel's salt solid solutions or physically onto calcium-silicate-hydrate surfaces). In these tests the process is non-steady-state: the progressive ingress of chlorides leads to variations of chloride concentrations and chloride binding as a function of depth and time (see a typical chloride profile in Fig. 1a). In contrast, a steady-state chloride ingress occurs after chlorides have reached the full depth of the sample, when the chloride binding capacity has been exhausted and the concentration profile in the sample remains constant over time.

In bulk diffusion tests, chloride profiles are measured after pre-determined exposure times (months to years) and they are generally interpreted in terms of apparent chloride diffusion coefficients, D_{app}. These coefficients are obtained by least-square fitting of chloride profiles with a simple solution of Fick's second law of diffusion (keeping all parameters constant and assuming the concrete specimen to be semi-infinite). These D_{app} combine in a single value the effects of chloride diffusion and chloride binding, while significantly simplifying the chloride ingress problem (e.g., D_{app} is not an intrinsic property and it reduces with exposure time). Nevertheless, different empirical approaches have been developed to use D_{app} as the main input for service

* Corresponding author.
E-mail address: william.wilson@usherbrooke.ca (W. Wilson).

https://doi.org/10.1016/j.cemconres.2020.106264
Received 3 July 2020; Received in revised form 1 October 2020; Accepted 9 October 2020

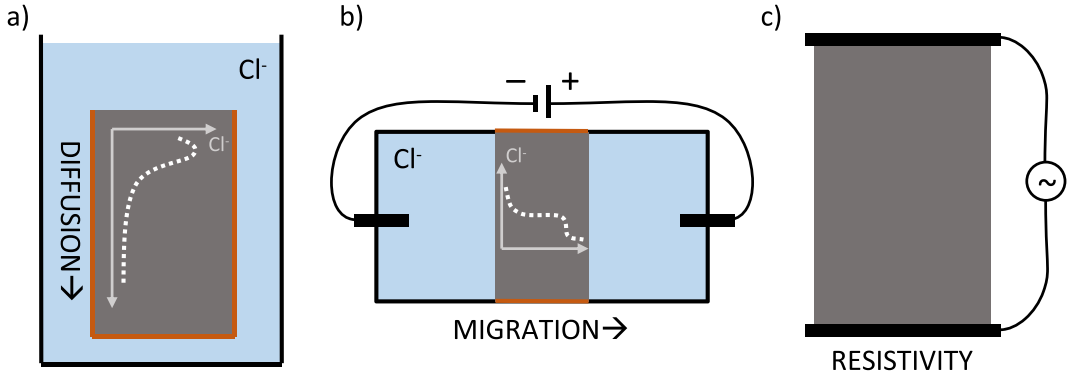

Fig. 1. Schematic representations of (a) a bulk diffusion test, (b) an electrically accelerated migration test, and (c) a bulk resistivity/conductivity test.

life predictive models based on Fick's laws. For example, the changes of D_{app} over time may be extrapolated with a multiplication factor called the aging factor, e.g., [7–12]. However, by combining different parameters of chloride ingress into single D_{app} values, this approach limits the understanding of mechanisms responsible for transport properties. Moreover, previous studies have shown the complexity of linking D_{app} to microstructure properties, such as the porosity, the chloride binding or the pore solution composition [10,13].

Notably, Hemstad et al. [14,15] showed the major influence of the pH on the chloride binding capacity and, by extension, on the chloride penetration profiles in solids (used for the calculation of D_{app}). The capacity of the paste to bind chlorides is a complex function of phase assemblage and chloride concentration as a function of depth, pH and leaching. Separating chloride diffusion and binding from a bulk diffusion test remains a challenge even when individual characterisation experiments are available [16]. This separation may not be critical for Ordinary Portland Cement (OPC) systems, but it is of great importance for understanding and predicting the effect new cementitious materials on chloride ingress.

Another limitation of the bulk diffusion test is the resource and time requirements, e.g., obtaining aging factors require years of exposure [11]. As schematized in Fig. 1b, accelerated tests were developed to rapidly assess chloride migration in a day or less (by forcing chlorides into the sample with electrical potential between two reservoirs). The most commonly used test methods are the rapid chloride permeability test (RCPT, ASTM C1202 [17]) and the rapid chloride migration test (RMT, NT Build 492 [18]). In the RCPT, the charge passed through the sample, Q, is measured at a fixed voltage for 6 h, and it is used as an indicator of the resistance to chloride penetration. In the RMT, a non-steady-state migration diffusion coefficient, D_{nssm}, is determined after about 24 h of test by measuring the penetration depth of the chloride front (a typical chloride front is shown in Fig. 1b). For engineering purposes, these tests are used to qualify concrete mixes for different exposure classes, e.g., ranges of charge passed Q in the Canadian standard [19] or D_{nssm} values in the Swiss standard [20].

From a scientific perspective, the characterisation of chloride ingress with apparent diffusion/migration test at the scale of concrete incorporates the effects of several parameters as schematized in Fig. 2. To better understand the underlying mechanisms and to enable long-term predictive performance modelling, it is important to decouple the different parameters. They can be grouped into four categories: concrete-scale effects, chloride binding, porosity, and pore solution.

1.2. From resistivity/conductivity of concrete to pore connectivity/tortuosity

The simplest way to remove the non-steady-state effects (i.e., chloride fronts and chloride binding) is to use an experimental approach without chlorides. Measurements of electrical resistivity/conductivity have thus gained interest in the last decade, either in terms of surface measurements [21] or bulk measurements [22] as schematized in Fig. 1c. The electrical resistivity is the capacity of a system to prevent the flow of electrical current, and the conductivity is its inverse. These very rapid methods were found to correlate well with RCPT results in several studies [3,23–26]. This correlation between the two tests is very useful, as it supports the replacement of the "relatively complex" (and criticized) RCPT by a resistivity test done in a few seconds (after about a week of specimen conditioning). Resistivity values equivalent to chloride penetration resistance classifications from RCPT have also been proposed [23]. From a mechanistic perspective, the correlation between these two tests (with and without chlorides) suggests that RCPT results are not significantly affected by chloride binding and by the non-steady-state nature of the test.

Electrically accelerated tests measuring chloride penetration not only depend on microstructure features (i.e., the "paths" for chloride diffusion), but also on the ionic strength of the solution, which governs its conductivity. The conductivity of the pore solution was found to vary by factors up to 2–3 between systems incorporating different cements and supplementary cementitious materials [27,28]. Reductions of conductivity of up to an order of magnitude were also observed with novel low-clinker materials, such as limestone calcined clay cement (LC^3) systems [29].

To decouple the first order effects of the pore solution, the resistivity of bulk concrete (ρ_b) is divided by the resistivity of its pore solution (ρ_0) to obtain the formation factor F. This factor may also be expressed in terms of conductivities (σ_0/σ_b) and it was also defined as the reciprocal of the product of the porosity (ϕ) and a pore connectivity parameter (β), following the approach originally postulated by Archie for oilfield rocks [30–32]:

$$F \equiv \frac{\rho_b}{\rho_0} = \frac{\sigma_o}{\sigma_b} \cong \frac{1}{\phi\beta} \quad (1)$$

Interestingly, the formation factor F was found to be related to the charge passed Q in the RCPT [33]. RCPT classifications were also translated into equivalent F values [32]. The formation factor approach has the advantage that it can be included in service life models using the Nernst-Einstein relationship [32], possibly combined with chloride binding [34]. However, this brings an important question about the pore solution and chloride ingress: should the effects of the pore solution be normalized out of bulk conductivity measurements (formation factor approach) or not (bulk conductivity approach), if both can be correlated to RCPT?

In addition, proposals have been made to relate the formation factor to descriptors of the porous network, either with a pore connectivity parameter β or with a tortuosity parameter τ. Depending on the approach, this latter term has been defined in terms of electrical/diffusion/geometrical tortuosity with variable definitions, such as $F = \tau/\phi$ (i.e., the inverse of β) [35–37] or [38–40] where higher values mean more complex (i.e. less linear) porous networks. Tortuosity has also

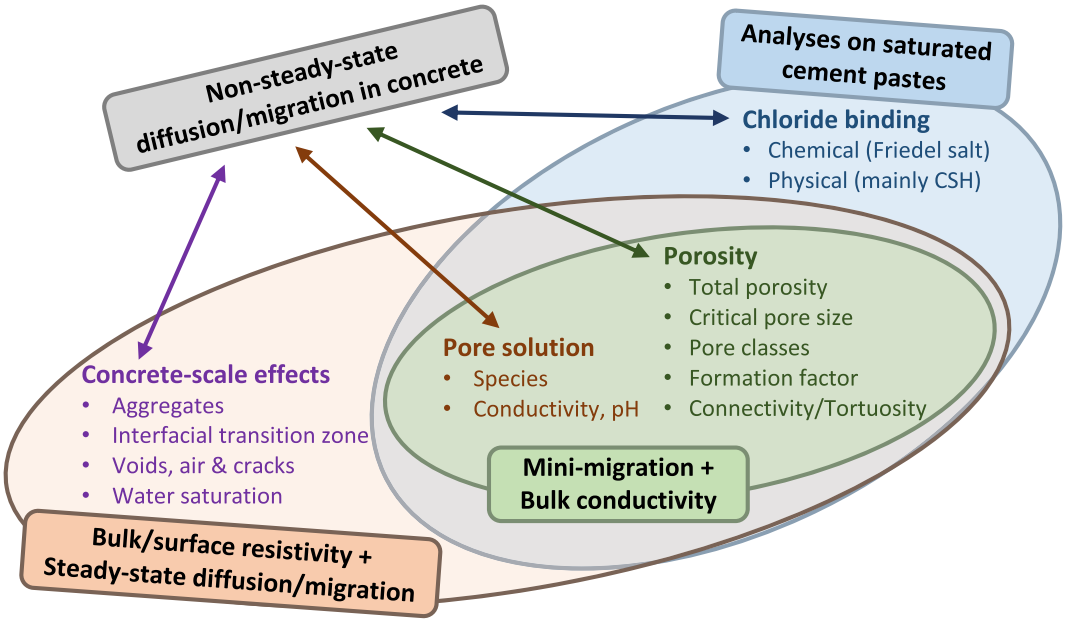

Fig. 2. Key parameters of chloride penetration with a schematic representation of the parameters included in different types of experimental tests.

been defined inversely or without considering the porosity (see, for example [41,42]), and the same quantity is also sometime defined as "macroscopic/microscopic geometrical parameters" [43] to avoid the over-interpretation usually attributed to the tortuosity.

Similarly as for ρ_b and F, relationships between tortuosity τ and accelerated chloride tests have been found (e.g., with the rapid chloride migration test in [40]). Once again, this type of relationships (observed between non-steady-state tests involving chloride binding and measurements based on electrical conductivity without chlorides) questions the role of chloride binding in accelerated tests. Moreover, it becomes difficult to determine which parameter (ρ_b, F, τ or β) should be correlated to which chloride ingress coefficient/indicator. Should the pore solution conductivity and the porosity be decoupled from the bulk conductivity measurements? One aim of this study is to explore these questions and relationships.

In addition, pore connectivity and tortuosity parameters can be seen as descriptors of the porous network, but they should be interpreted carefully [31] as the contribution of each phenomena/mechanism hiding in these parameters is still unclear (e.g., effects of the geometry of the pore network, interactions between ions and surfaces, errors from conductivity or porosity measurements, etc.). Moreover, the concept of electrical/diffusion tortuosity is sometimes associated to geometrical tortuosity, suggesting that the porous path is τ times longer than a straight path. However, this association should be avoided as the very high values obtained for cement pastes and concrete (e.g., $\tau > 100$ [35]) have not yet been explained by geometrical properties of the porous network [44]). For that reason, the pore connectivity and tortuosity parameters in cement paste should be interpreted as the unexplained component of the bulk conductivity once the linear effects of the pore solution conductivity and the porosity have been removed.

1.3. Steady-state chloride diffusion/migration in concrete

Another approach to study chloride diffusion while avoiding the effects of binding is to investigate the effective diffusion under a steady-state regime (after the chloride binding capacity has been exhausted) by the direct or indirect measurement of the chloride ion flow through the sample. As natural diffusion is a very slow process compared to the characteristic size of concrete (requiring years of testing), electrically accelerated migration tests are a much faster alternative. The standardized method NT Build 355 [45] describes a steady-state migration method. The samples are placed between an upstream reservoir with chlorides and a downstream reservoir without chlorides. An external voltage is applied between the two reservoirs to force the chloride movement from upstream to downstream. The setup is very similar to that of non-steady-state tests of Fig. 1b, but the effective diffusion coefficient is estimated from the chloride flow through the sample (after chloride breakthrough in the downstream reservoir). The flow is measured by sampling the downstream reservoir at periodic interval and titrating with silver nitrate titration. The diffusion is then calculated from migration results using a simplification of the Nernst-Planck equation, as suggested by Andrade [46].

The approach was further investigated and validated [43,47–51]. Marchand and co-workers patented a modified migration test setup [52] solving specific problems of previous setups. In this test, the chloride flow is not directly measured, but the evolution of the migration current is monitored over a period of 14 days. Effective diffusion coefficients are then back-calculated from current curves using their reactive transport model STADIUM® [49,52] along with characteristics of the concrete microstructure (the porosity, the estimated phase assemblage and the capacity to bind chloride). These coefficients can then be validated with non-accelerated bulk diffusion tests using the same model. They can then be used for engineering purposes to predict the service life of reinforced concrete elements. However, the development of novel alternative binding systems (e.g., limestone-calcined-clay cements, LC^3) generates new challenges in terms of understanding and modelling [16], due to a higher degree of complexity linked to the phase assemblage and interactions with chlorides [53]. This brings the needs for a better understanding and decoupling of chloride ingress mechanisms, which is an underlying motivation for the approach proposed in this paper.

1.4. Combining approaches: mini-migration in saturated cement pastes

The proposed mini-migration approach focusses on the measurement of "steady-state" processes in saturated cement pastes to remove the complexity associated with macro-scale effects and chloride binding (see Fig. 2). The prefix "mini" refers to the cement-paste scale of the setup and samples, instead of the mortar or concrete scales commonly investigated with diffusion/migration methods. The approach uses the mini-migration setup as a central method along with complementary experimental techniques to investigate the same cement pastes before,

during and after mini-migration. The combination of techniques not only provides a migration current curve and an effective diffusion coefficient from the flow of chloride, but it also enables a comprehensive characterisation of the samples in terms of: the microstructure (e.g., with mercury intrusion porosimetry), the phase assemblage and chemically bound chlorides (with X-ray diffraction), elemental and phase profiles (with scanning electron microscopy and energy-dispersive X-ray mappings image analysis, *edxia* [54]), and the composition and conductivity of the pore solution.

More specifically, this study explores relationships between the effective diffusion coefficient, the porosity, the pore solution conductivity, the bulk conductivity, the formation factor and the pore connectivity parameter. As described above, chloride ingress has previously been correlated with these different parameters although all the reported correlations cannot be simultaneously universal. To unravel links between these parameters, this study investigates a range of blended-cement pastes and water-to-binder ratios sufficiently wide to avoid system-specific correlations based on an incomplete dataset. Moreover, the effect of each binder type on the different parameters is examined.

2. Materials and methods

2.1. Materials

This study compares six different types of binder including three commercial cements: a CEM I 42.5N Ordinary Portland Cement (OPC), a White Portland Cement (WPC), a slag-Portland blended cement with 60% slag (CEM III/A). Two other systems are binary blends of the same CEM I with variable proportions of supplementary cementitious materials (SCMs): a mixture of 20% class F fly ash and 80% CEM I (20%FA), a mixture of 20% glass powder and 80% CEM I (20%GP). The last system is a limestone calcined clay cement with 50% of Portland clinker (LC^3-50), which was produced by mixing 53% of CEM I, 30% of calcined clay (fired and ground in India, with a calcined kaolinite content of ~45%), 15% fine commercial limestone powder and 2% chemical-grade gypsum. Table 1 shows the chemical composition of the materials as measured by X-ray fluorescence.

2.2. Sample preparation and curing

Cement pastes were prepared by mixing the different binders with distilled water at water-to-binder ratios of 0.3, 0.4 and 0.5. The mixing method was defined with the aim to ensure the homogeneity and the representativeness of the relatively thin samples (~1 cm) and to avoid misinterpretations due to defects or air bubbles.

For the laboratory-blended binders, the powders were pre-homogenised with a Turbula blender for 10 min in 1 L containers (500–800 g of powder with 4 ceramic balls of ~3 cm diameter). After the addition of water, the pastes were mixed for 2 min with a 5 cm axial-flow impeller at 1600 rotations per minute. This high-shear mixing was followed by 1 min of vacuum mixing at 450 rotations per minute to remove entrapped air. At lower water-to-binder ratios, a polycarboxylate-based superplasticizer was used when necessary to obtain sufficient workability for casting. At higher water-to-binder ratios for some binders requiring less mixing water, bleeding was prevented by adding a waiting time between the high-shear and vacuum mixing steps (e.g., 1 h for 20%FA system at w/b = 0.4). Although this approach may be detrimental for early-age hydration, it was found to be the best way to obtain pastes with water porosities higher than the limit imposed by bleeding. After mixing, pastes were cast in cylindrical polypropylene moulds of 33 mm diameter, which remained sealed for the first 20 h before demoulding. They were then water-cured for 28 days in slightly larger containers to limit volumes of curing water. A sacrificial, finely-ground specimen of the same batch was also added to each container to

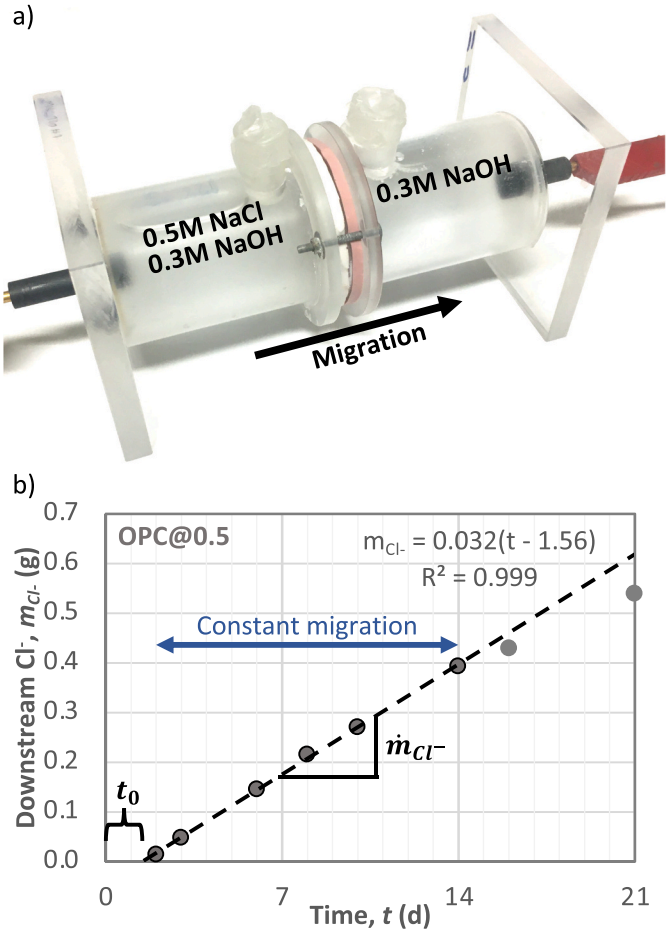

Fig. 3. (a) The mini-migration setup for accelerated migration of chlorides from the upstream reservoir to the downstream reservoir, through a cement paste specimen of 33 mm diameter and 10 mm thickness. (b) The mass of chlorides in the downstream reservoir as a function of time, as obtained for the OPC system at w/b = 0.5 from $AgNO_3$ titration of 5 mL solutions sampled periodically (following an initial breakthrough time t_0, a constant migration regime is obtained until the change of concentration in the reservoirs becomes non-negligible, e.g., after ~14 days in this figure).

Table 1
The chemical composition (mass %) of cements and SCMs used in this study (LOI is the Loss Of Ignition).

Material	Na_2O	MgO	Al_2O_3	SiO_2	SO_3	K_2O	CaO	TiO_2	Fe_2O_3	LOI
CEM I	0.4	1.1	5.4	20.7	2.9	0.7	65.0	0.2	1.9	1.8
WPC	0.2	0.5	2.1	24.4	2.1	0.1	67.8	0.1	0.3	1.1
CEM III/A	0.4	4.3	7.2	27.5	4.2	0.8	52.9	0.5	1.2	0.6
Fly ash	0.8	1.3	23.5	57.3	0.2	2.5	2.3	1.3	6.7	3.5
Calcined clay	0.1	0.0	36.7	56.1	0.1	0.2	0.2	2.4	3.4	0.5
Limestone	0.1	0.2	0.0	0.1	0.0	0.0	56.2	0.0	0.0	43.4
Glass powder	13.2	0.9	1.6	70.8	0.1	0.6	10.7	0.0	0.3	1.1

protect the sample from leaching and to approach the curing of specimens in their own pore solutions.

2.3. The mini-migration setup for pastes

As shown in Fig. 3a, mini-migration experimental setups were fabricated following a similar design as the chloride migration setup developed by Marchand et al. [52]. However, the two approaches differ by their size. Dimensions of setups in this study are ~1/30 those of the concrete-scale migration setups. Downscaling the setup dimensions enabled easier testing at the scale of the cement paste, using disc specimens of 33 mm diameter by 10 mm thickness with reservoirs of about 125 mL.

After cutting and polishing surfaces, the cylindrical surface of specimens was coated with silicon, which was also used to mount the sample on a plastic ring. After coating, the mounted samples were immersed for 48 h in a 0.3 M NaOH solution under slight vacuum. The inner diameter of the plastic ring is 30 mm (slightly smaller than the sample to avoid leaks) and the ring is held between the two reservoirs with screws and rubber seals. The upstream reservoir is filled with a solution of 0.5 M NaCl and 0.3 M NaOH, whereas to the downstream reservoir contains a 0.3 M NaOH solution to limit leaching of alkalis. During the period of the test, a fixed voltage was applied with a benchtop direct current generator to force chlorides through the specimen towards the downstream reservoir. The voltage was adjusted for each binder type (e.g., 5 V for OPC systems) in order to reach an initial migration current between 10 and 20 mA. This current resulted in tests of adequate duration (2–3 weeks) and was compatible with the logging instrument (Squirrel Data Logger, Grant Instruments) which continuously monitored the migration current during the test. In addition, the electrical potential between reservoirs was measured regularly with a handheld multimeter.

The flow of chlorides through the specimen was then measured by sampling the downstream reservoir every 2–4 days. The chloride concentration was titrated with a TitroLine® 5000 using a 0.05 M $AgNO_3$ solution. Fig. 3b shows a typical result of the chloride mass in the downstream reservoir as a function of time (for the OPC system at $w/b = 0.5$). At the beginning of the test, the chloride front progressively penetrates through the depth of the specimen, saturating on the way the binding capacity of the cement paste (both in terms of chemical and physical binding). The breakthrough time t_0 is the moment where chlorides begin exiting the sample into the downstream reservoir, which is a complex function of experimental parameters, transport properties and chloride binding capacity. The flow of chloride through the specimen is then stable during the constant migration regime the duration of which depends on the chloride flow (a higher flow leads to a shorter constant migration regime). Nevertheless, after some time (e.g., 14 days in Fig. 3b), concentrations and conditions change sufficiently that the flow of chloride is no longer constant.

By considering the chloride flow during the constant migration regime, the effective chloride diffusion coefficient, D_{eff}, can be estimated using an analytic approach based on the Nernst-Planck equation [55] for transport processes in solution:

$$J_{i,e} = -D_{i,e}\left(\frac{\partial c_i}{\partial x} + c_i\frac{z_i F}{RT}\frac{\partial U}{\partial x} + c_i\frac{\partial ln(y_i)}{\partial x}\right) \quad (2)$$

where the flux $J_{i,e}$ of species i is function of the diffusion coefficient $D_{i,e}$ and contributions from three terms related to diffusion, migration and non-ideal diffusion (c_i is the concentration, z_i the electrical charge, y_i the activity coefficient, U the electrical potential, F Faraday's number, R the gas constant, and T the absolute temperature).

As proposed by Andrade [46], the equation can be simplified in the case of a chloride migration experiment. First, the contribution of diffusion is neglected compared to the electro-migration flux. In addition, since the samples are considered fully-saturated, advection is also neglected. Second, the constant migration regime is considered quasi steady-state: the flux of chloride is constant (i.e., the concentration in the downstream reservoir is increasing linearly after breakthrough, see Fig. 3b) and the variation of concentration in the upstream reservoir is neglected. Third, the local electric field between surfaces and ionic species in the pore solution (e.g., OH^- Cl^-, Na^+, K^+, etc.) is neglected compared to the external voltage. In addition, the voltage loss in the solution is assumed to be null. With these assumptions, a constant electric field through the cement paste can be obtained by dividing the voltage (measured near the specimen) by the specimen thickness. Finally, the influence of non-ideality of the solution is neglected and the chemical activities are assumed to be equal to the concentration (as in, e.g., NT Build 355 [45]). Considering the above assumption and simplifications, the Nernst-Planck equation can be rewritten as:

$$D_{eff} = \frac{J}{c_{up}}\frac{RT}{F}\frac{l}{\Delta E} \quad (3)$$

where D_{eff} is the chloride effective diffusion coefficient (after the effects of binding have been exhausted), R is the gas constant, T is the temperature [K], F is the Faraday constant, l is the specimen thickness [m], c_{up} is the chloride concentration in the upstream reservoir [mol/m^3], ΔE is the voltage drop across the specimen [V], and J is the chloride flux through the specimen [mol/m^{2}s]. Experimentally, J can be determined from the slope $\dot{m}_{Cl^-}$ [g/s] of the chloride mass in the downstream reservoir as a function of time:

$$J = \frac{\Delta c_{down} V_{down}}{\Delta t A} = \frac{\dot{m}_{Cl^-}}{M_{Cl^-} A} \quad (4)$$

where Δc_{down} is the variation of the chloride concentration in the downstream reservoir [mol/m^3] per time interval Δt [s], V_{down} is the volume of the downstream reservoir [m^3], A is the specimen surface area [m^2], and M_{Cl^-} is the molar mass of chlorine [g/mol].

2.4. Complementary characterisation of the cement pastes

The water porosity, ϕ, was estimated from the relative volume of water that can be removed by freeze drying, similarly as in [51]. This method was preferred to the approach of drying and resaturation under vacuum, because our water-cured specimens were already as close as possible to complete saturation (they were never dried) and to avoid artefacts due to pore collapse and microcracking during the drying of cement pastes. For each system, 3 slices of 33 mm diameter and ~2 mm thickness were cut (under water), weighted in a saturated surface dry condition, and their dimensions precisely measured with a calliper. Water was removed by freeze-drying with a 10 min immersion in liquid nitrogen followed by 48 h in the freeze dryer under a vacuum of ~0.08 mbar. The dried samples were reweighted and then the water porosity was calculated by mass loss difference. This water porosity is expected to be higher than the porosity measured by MIP, as the latter does not include the very fine pores [56].

The bulk resistivity, ρ_b, of the cement pastes was directly measured with a method adapted from ASTM C1876 [22] for cement pastes cured in their own pore solution. After calibration, a Giatec RCON^2 instrument was used at 1 kHz on cylindrical cement paste specimens of 33 mm diameter by ~50 mm length, using smaller electrodes fabricated as downscaled replicates of the RCON^2 electrodes for concrete. The bulk conductivity, σ_b, is the inverse of the bulk resistivity $\sigma_b = 1/\rho_b$.

The conductivity of the pore solutions, σ_0, was directly measured with a Mettler Toledo conductivity probe (after calibration with a 1413 μS/cm standard solution). The pore solutions were obtained by extraction from cement paste samples using an experimental setup similar to that proposed by Barneyback and Diamond [57]. A loading ramp of 5 min was used to reach a stress of 570 MPa and the pressure was kept up to 10 min (depending on w/b, to obtain at least 3 mL of pore solution).

The critical pore entry radius, r_{crit}, was obtained from the maximum of the derivative of the pore entry radius distribution obtained by mercury intrusion porosimetry. After drying by solvent exchange (more

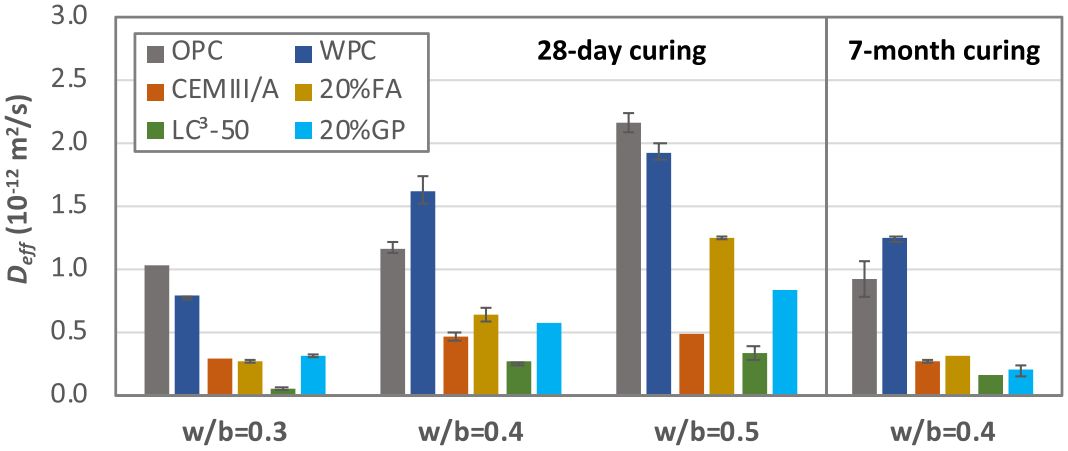

Fig. 4. Effective chloride diffusion coefficients, D_{eff}, measured from chloride flows in mini-migration tests on blended-cement pastes at different water-to-binder ratios. The error bars illustrate the standard deviation between replicates.

than 7 days in isopropanol with 3 solvent renewals), about 1 g of a cement paste sample was placed into the dilatometer (5 pieces with a thickness of ~2 mm). The pore entry radius distributions were obtained by combining results from Pascal 140 and Pascal 440 instruments (up to a pressure of 400 MPa), assuming a contact angle of 140°.

3. Results and discussion

3.1. Diffusion coefficients from mini-migration

Fig. 4 shows chloride effective diffusion coefficients, D_{eff}, measured with the mini-migration test at the ages of 28 days and 7 months for the 18 systems of interest (6 binder types at 3 different *w/b*). As expected, an increase of D_{eff} was observed for each binder type with the increase of *w/b*. More interestingly, for each *w/b*, a significant reduction of D_{eff} was observed for all types of blended-cement systems compared to OPC & WPC systems. Fig. 4 also presents D_{eff} measured on samples at $w/b = 0.4$ after 7 months of curing, which shows non-negligible reductions of D_{eff} compared to measurements at 28 days (notably for 20%FA and 20%GP systems which clearly had not developed their full potential at 28 days).

Among all the tested systems, the LC^3-50 systems stand out as they reach rapidly the lowest D_{eff} values. At 28 days, values at $w/b = 0.5$ are in the same range as the other blended-cement systems at $w/b = 0.3$. This difference tends to diminish with longer curing time, as systems like 20%GP catch up after 7 months. Fig. 4 not only enables the comparison of new types of binders,the measured D_{eff} values can also be used as inputs for transport modelling and for further investigation of mechanisms. The interpretation and understanding of the particularities of each system require complementary characterisation.

3.2. Range of microstructural characteristics of the investigated binders

The investigated blended-cement binders were chosen with the aim to find general relationships between D_{eff} and microstructure features. Conventional and alternative supplementary cementitious materials were chosen to cover a wide range of properties in terms of porosity, pore solution conductivity and bulk conductivity.

As shown in Fig. 5a, microstructures of pastes at $w/b = 0.3$, 0.4 & 0.5 have water porosities ranging from ~20% to ~45% (as measured by freeze-drying, see Materials and methods). In general, the variation of *w/b* had a larger impact on the water porosity than the type of binder (for the same *w/b*). On the contrary, the binder type had a greater influence than *w/b* on the conductivity of the pore solution (σ_0), as also shown in Fig. 5a. The pore solution of WPC and LC^3-50 systems have much lower alkali and hydroxyl contents (i.e., lower conductivity) compared to the other systems. WPC clinker have a naturally low alkali content (see Table 1), and the LC^3-50 mix contains only 50% of clinker with alkalis and those are likely to be bound to a higher degree by C-(A-)S-H with a lower Ca/Si ratio [58,59]. Furthermore, a decrease of pore solution conductivity was observed with the increase of *w/b*, which was explained by dilution: for a similar hydration degree, the alkalis released in the pore solution are similar but the pore solution volume is higher for higher *w/b*. Overall, the measured pore solution conductivity for OPC and CEMIII/A systems are in a range similar to previously reported values by other authors [60].

Fig. 5b shows the same systems in the axes of pore solution conductivity (σ_0) vs. bulk conductivity ($\sigma_b = 1/\rho_b$, i.e., the inverse of bulk resistivity). As the bulk conductivity of the paste depends on the conductivity of the pore solution, those parameters may be expected to be correlated, as seen with "conventional" blended-cement systems. For each *w/b*, the OPC system (high σ_0, high σ_b) and the LC^3-50 system (low σ_0, low σ_b) are endpoints of the correlation, with 20%FA and CEMIII/A systems agreeing to some extent with the expected trend. However, WPC and 20%GP systems do not align with the other systems in terms of relationship between bulk conductivity and pore solution conductivity (low σ_0, high σ_b for WPC; high σ_0, low σ_b for 20%GP), which broadens the range of values covered. The contribution of other parameters influencing bulk conductivity are further investigated below (e.g., effects of binders on the pore network).

3.3. Binder-specific correlations between the effective diffusion coefficient, the pore network and the pore solution

To explore possible correlations between effective chloride diffusion coefficients and microstructure parameters, Fig. 6a shows D_{eff} as a function of the water porosity. For each binder type, the increase of *w/b* leads to the increase of both the porosity and D_{eff}. This expected result can be explained by the increase of the water porosity, which leads to wider paths for chloride flow. However, there is no general relationship between the water porosity and D_{eff} when considering different types of binder, as also previously observed with other chloride ingress tests [16,31,61]. This result indicates that the binder type has more impact on D_{eff} than the water porosity.

Fig. 6b illustrates the effects of the pore network by showing D_{eff} as a function of the critical pore entry radius, as determined by MIP. Because MIP is a time-consuming method, the dataset was limited to 3 binder types. This was sufficient to illustrate that the critical pore entry radius cannot be directly linked to the variation of D_{eff} for different binder types at the same *w/b* (as in [16]). Similar D_{eff} were obtained for OPC and WPC systems, although the critical pore entry radius of the latter was about 50% higher.

Fig. 6c suggests that the pore solution conductivity is unrelated to D_{eff}, when comparing all the investigated binders. For example, the same $D_{eff} \approx 0.3 \times 10^{-12}$ m^2/s can be obtained with $\sigma_0 = 5$–20 S/m.

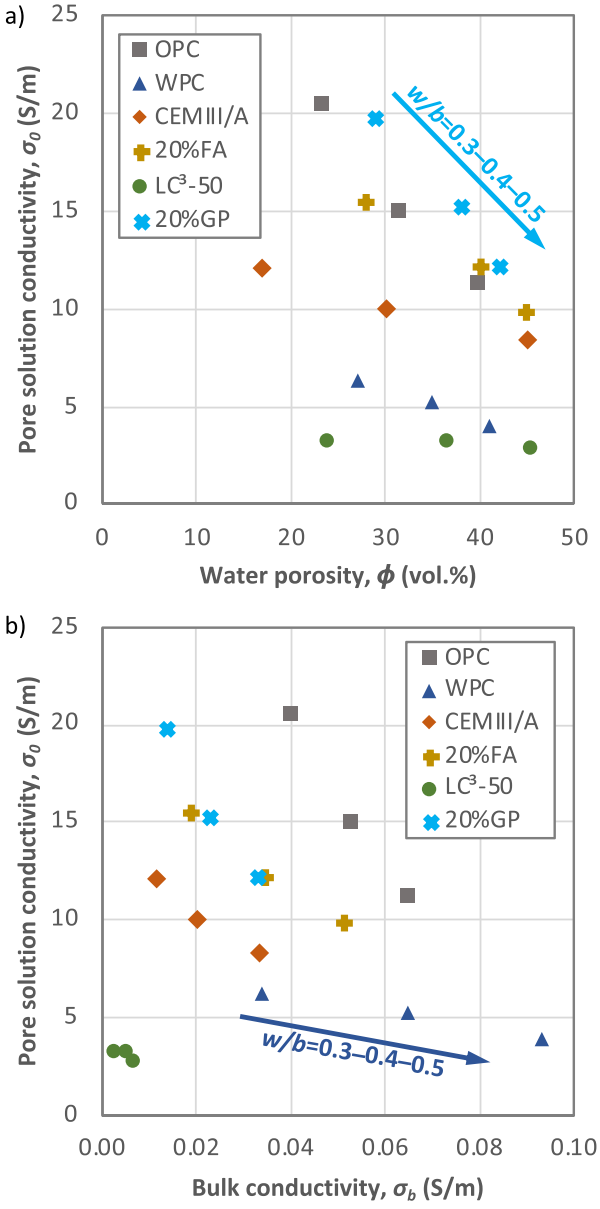

Fig. 5. The investigated systems cover a wide range of properties in terms of pore solution conductivity vs. (a) water porosity and (b) bulk conductivity.

Moreover, the trend for each binder appears counterintuitive: a higher pore solution conductivity is the indication of a higher ionic concentration in the pore solution (mainly alkalis and hydroxyls) that would be expected to facilitate chloride ingress through ionic exchange with hydroxyls. However, lower D_{eff} values obtained for systems with higher pore solution conductivites indicates that the effects of the pore network (i.e., lower w/b) dominate the effects of pore solution conductivity on chloride effective diffusion.

3.4. General correlation between the effective diffusion coefficient and the bulk conductivity

While there was no simple correlation between the effective chloride diffusion and the water porosity or the pore solution conductivity, a general relationship was observed between D_{eff} and the bulk conductivity, as shown in Fig. 7a. Notably, the correlation between these parameters is quite strong with $R^2 = 0.83$, with a trendline crossing the origin (without forcing any intercept value).

The value of the OPC system at $w/b = 0.5$ is considered an outlier.

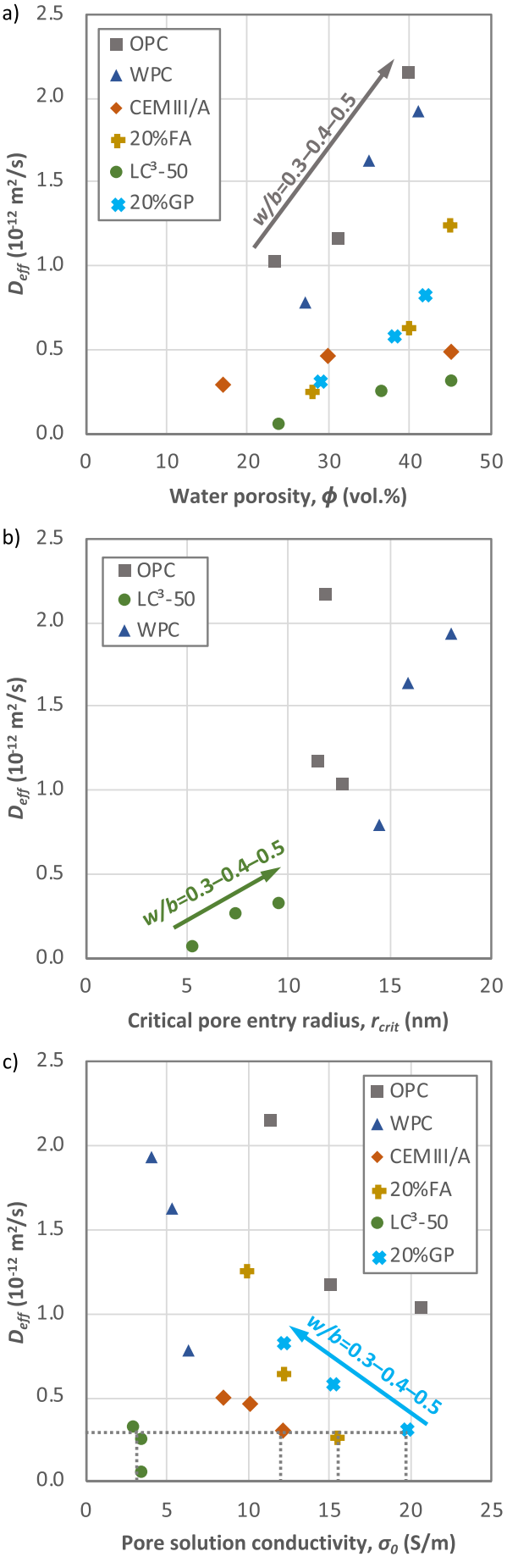

(caption on next page)

Fig. 6. Effective diffusion coefficient, D_{eff}, as a function of (a) water porosity, (b) critical pore entry radius, and (c) pore solution conductivity, showing binder-specific correlations between D_{eff} and w/b, but no general relationship including all the binder types (e.g., the same $D_{eff} \approx 0.3 \times 10^{-12}$ m^2/s can be obtained with σ_0 = 5–20 S/m).

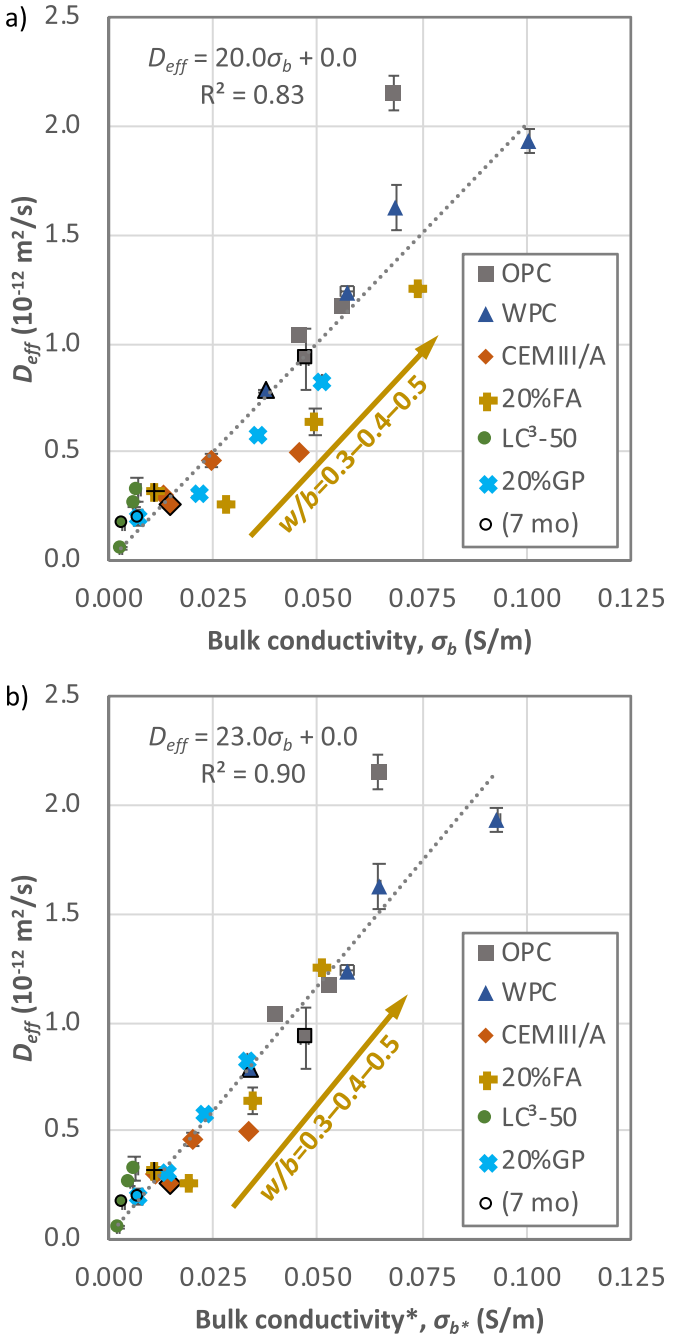

Fig. 7. General relationships between the effective diffusion coefficient, D_{eff}, and (a) the bulk conductivity at 28 days or (b) the adjusted bulk conductivity* (the average between 28-day and 91-day results), which considers microstructure changes occurring during the mini-migration test.

The points falling below the trendline can be explained by the evolving microstructure of blended-cement systems during the mini-migration test at 28 days (e.g., 20%FA or 20%GP). The bulk conductivity is an instantaneous measurement at 28 days. However, the mini-migration lasts ~14 days during which SCMs continue to react, leading to the measurement of D_{eff} values lower than those exactly at 28 days. This observation is supported by 7-month results which are much closer to the trendline (see markers with black contour in Fig. 7a), because the microstructure is no longer evolving significantly between the two tests.

The evolution of the microstructure during the mini-migration test is further supported by Fig. 7b, where each bulk conductivity* value is the average between 28-day and 91-day results (bulk conductivity was not measured in between). The correlation in Fig. 7b is even better with R^2 = 0.90, as slowly reacting blended-cement systems join the other systems on the same trendline. These two tests may be used as indicators of the effective chloride diffusion in cement pastes. However, the mini-migration has the advantage of providing a diffusion coefficient, which is required for chloride transport modelling.

Bulk conductivity (or bulk resistivity) has been previously correlated with other chloride ingress indicators evaluating transient regimes, such as the rapid-chloride permeability test or the bulk diffusion test. Nevertheless, the correlations of Fig. 7 confirm that the diffusion measured by mini-migration is not influenced by chloride binding (there is no chlorides involved in bulk conductivity measurement). Furthermore, they stress the importance of testing chloride ingress at later age because of the microstructure evolution after 28 days for slowly reacting blended-cement systems.

3.5. Relationships between the effective diffusion coefficient, the formation factor and the pore connectivity parameter

As described previously with Eq. (1), the bulk conductivity can be combined with other measurements to describe the structure of the porous network with parameters such as the formation factor F or the pore connectivity parameter β. As shown in Fig. 8a and b, the WPC pastes clearly fall off the trend shown by the other samples, which limits any general relationship between D_{eff} and the formation factor or the pore connectivity parameter. Fig. 8c further illustrates the particularity of the WPC systems, which have a similar range of water porosity as the other systems, but much higher pore connectivity values (although D_{eff} is in the same range as that of OPC pastes). This observation with WPC is of great importance as it confirms that the structure of the porous network is not sufficient to predict diffusion, and that the properties of pore solution have to be taken into account.

3.6. Discussion on key parameters affecting the effective diffusion coefficient

The comparison of a wide range of blended-cement systems at different w/b provides a better overview of the influence of different parameters on the effective chloride diffusion coefficient:

- Firstly, for a specific binder type, a lower water porosity (i.e., lower w/b) leads to a lower D_{eff} value (see Fig. 6a);
- Secondly, lower values of the pore connectivity parameter correspond to lower D_{eff} values. For example, OPC and 20%GP systems at the same w/b have similar pore solution conductivities (see Fig. 6c) but the 20%GP system has significantly lower values of the pore connectivity parameter and D_{eff} (see Fig. 8b).
- Thirdly, a lower pore solution conductivity generally leads to a lower D_{eff} value, as illustrated by comparing 20%GP and LC^3-50 systems at w/b = 0.4: both systems have a similar water porosity and pore connectivity parameter (see Fig. 8c), but the LC^3-50 system has a much lower pore solution conductivity and D_{eff} (see Fig. 6c).

The bulk conductivity and D_{eff} measurements depend on the combination of these three parameters, whereas the relative importance of each parameter vary from one system to the other. For this reason, it is of interest to decouple the different effects as illustrated by the diverse set of samples of this study. For example, OPC and WPC systems have similar ranges of D_{eff} although the relative importance of each parameter is different. WPC pastes have very high pore connectivity

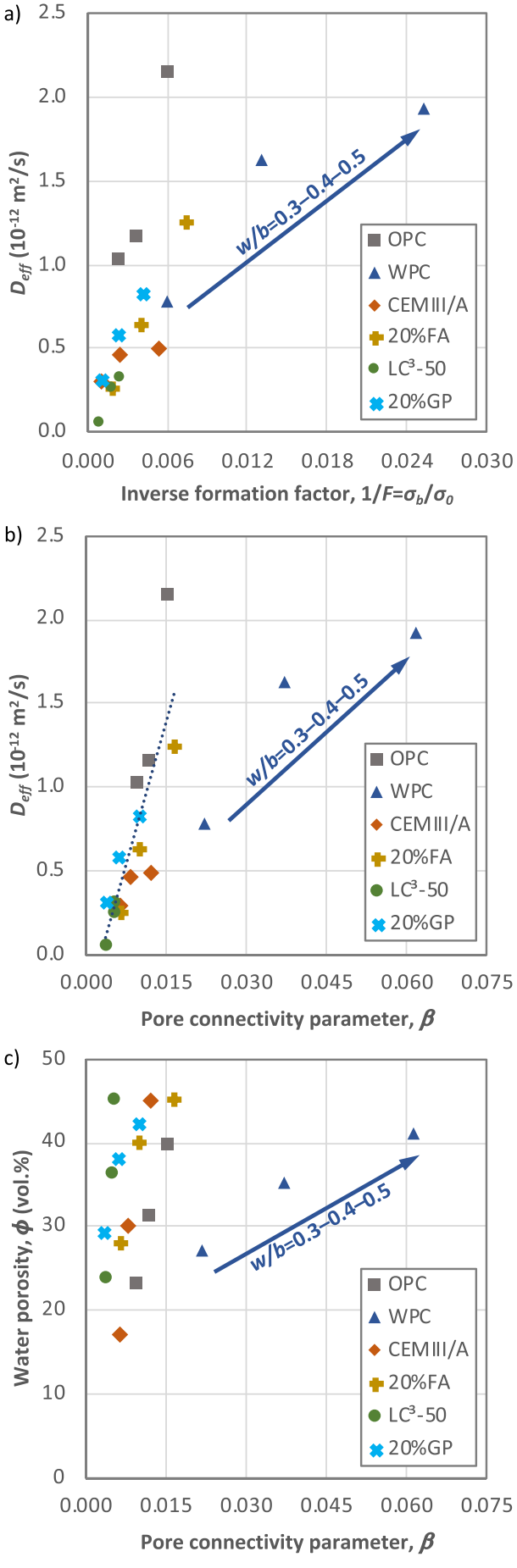

Fig. 8. Effective diffusion coefficient, D_{eff}, as a function of (a) inverse formation factor and (b) pore connectivity parameter; (c) water porosity vs. pore connectivity parameter.

parameters compared to OPC pastes (which should result in high D_{eff} values). Nevertheless, the pore solution conductivity of WPC systems is very low compared to that of OPC systems, which seems to compensate the higher pore connectivity values and to lead to D_{eff} values in the same range as those of OPC systems.

In addition, decoupling the different parameters explains the very low D_{eff} values for LC^3-50 systems. These systems have both the lowest pore solution conductivity and the lowest pore connectivity values of all investigated systems! These results further indicate that the relative impact of the water porosity (i.e. w/b) is very small compared to that of the other two parameters, as the LC^3-50 paste at $w/b = 0.5$ performs better than almost all investigated systems at lower w/b. The low conductivity of the pore solution can be explained by the reduced clinker content and the alkali binding in C-A-S-H with low Ca/Si. However, understanding the true physical meaning of the pore connectivity parameter in blended-systems is more complex as several mechanisms are aggregated in this parameter (e.g., disconnected porosity, effective w/b, surface interactions, and more). Although it is beyond the scope of this paper, an ongoing research further investigates these mechanisms.

Overall, most blended-cement systems behave similarly by reducing both the pore solution conductivity and the pore connectivity parameter values to different extents. The 20%GP systems are counter-examples. The dissolution of glass powder releases Na^+ ions and pore solution conductivities are similar or higher than those of OPC systems (as in [27]). Nevertheless, the very low D_{eff} measured for the 20%GP system after 7 months of curing indicates that the impact of the pore connectivity parameter on effective diffusion can be greater than that of any other parameter (at least for the investigated range of binders).

4. Conclusion

This study investigates chloride ingress at the scale of the cementitious binder with the mini-migration method (without concrete-scale effects and chloride binding, during a constant migration regime). A wide range of blended-cement pastes was investigated at $w/b = 0.3$, 0.4 & 0.5 to explore relationships between effective chloride diffusion coefficients (D_{eff}) and microstructure features (e.g., pore structure and pore solution). The wide selection of systems turned out to be critical, not only to avoid conclusions based on incomplete datasets, but also to reveal how each binder type resists chloride ingress by a different combination of mechanisms. The main findings can be summarized as follows:

- A general relationship was obtained between the effective chloride diffusion coefficient D_{eff} (measured by mini-migration) and the bulk conductivity σ_b. Both parameters can characterize the effective ingress of chloride (without effects of chloride binding), but D_{eff} has the advantage of being an input for chloride transport modelling.
- No simple relationship exists between D_{eff} and the formation factor F or the pore connectivity parameter β. The pore solution conductivity plays a significant role in diffusion. Therefore, bulk conductivity measurements should not be normalized by the pore solution conductivity.
- Chloride ingress was correlated with w/b for each binder, but the type of binder had a greater impact on D_{eff} because of its effect on the pore solution and on the pore network (different binders were also found to exhibit similar D_{eff} with very different microstructures, e.g., Portland and white Portland cements).
- The incorporation of supplementary cementitious materials in blended-cements pastes increased the resistance to chloride ingress

by reducing the pore connectivity parameter and/or the pore solution conductivity.

Overall, this study demonstrates that the mini-migration method is a powerful tool to understand transport properties and governing mechanisms at the scale of the binder and to develop novel ultra-durable binders.

The full potential of the method remains to be explored, as the method not only enables characterisation of the exact same cement paste before the mini-migration (e.g., porosity by MIP, phase assemblage by XRD, bulk conductivity, pore solution conductivity, etc.), but also during and after the mini-migration (e.g., chemical chloride binding by XRD, chloride profiles by μXRF, phase profiles by SEM-EDX/edxia [54], etc.). This comprehensive material characterisation at different stages of mini-migration experiments provides inputs and validations for reactive transport modelling of chloride ingress in novel cementitious systems. Ongoing research aims to gather comprehensive datasets for specific mixes to be used for benchmarking reactive transport modelling approaches, to develop a reactive transport model using such data, and to investigate the very-low pore connectivity measured in this study for cement pastes incorporating 20% glass powder and for limestone calcined clay cement pastes.

CRediT authorship contribution statement

William Wilson: Conceptualization, Methodology, Validation, Investigation, Writing - Original Draft, Funding acquisition.

Fabien Georget: Conceptualization, Methodology, Validation, Writing - Review & Editing.

Karen Scrivener: Conceptualization, Writing - Review & Editing, Supervision, Funding acquisition.

Declaration of competing interest

The authors declare that they have no known competing financial interests or personal relationships that could have appeared to influence the work reported in this paper.

Acknowledgements

The authors would like to thank the Fonds de recherche du Québec – Nature et technologies (FRQNT), for partial financial support to the first author for this research. The authors further acknowledge Julien Nicolas Gonthier, François Montuori, Manuel Piot and Kshitij Bansal for their contributions in the laboratory.

References

[1] G. Mailhot, The New Champlain Bridge – technical requirements and delivery status report, Can. Civ. Eng. 34 (2017) 22–25.
[2] K.D. Stanish, R.D. Hooton, M.D. Thomas, Testing the Chloride Penetration Resistance of Concrete: A Literature Review, (1997).
[3] Q. Yuan, M. Santhanam, Test methods for chloride transport in concrete, in: M. Alexander, A. Bertron, N. De Belie (Eds.), Perform. Cem. Mater. Aggress. Aqueous Environ. State-of-the-Art Report, RILEM TC 211 - PAE, Springer Netherlands, Dordrecht, 2013, pp. 319–343, , https://doi.org/10.1007/978-94-007-5413-3_13.
[4] C. Shi, Q. Yuan, F. He, X. Hu, Transport and Interactions of Chlorides in Cement-based Materials, CRC Press, 2019.
[5] NT BUILD 443, Concrete, Hardened: Accelerated Chloride Penetration, Nordtest, Taastrup, Denmark, 1995.
[6] ASTM, C1556-11a, Standard Test Method for Determining the Apparent Chloride Diffusion Coefficient of Cementitious Mixtures by Bulk Diffusion, ASTM International, West Conshohocken, PA, 2016.
[7] L. Tang, L.O. Nilsson, Chloride diffusivity in high strength concrete, Nord. Concr. Res. 11 (1992) 162–170.
[8] P.S. Mangat, B.T. Molloy, Prediction of long term chloride concentration in concrete, Mater. Struct. 27 (1994) 338, https://doi.org/10.1007/BF02473426.
[9] M.D.A. Thomas, P.B. Bamforth, Modelling chloride diffusion in concrete effect of fly ash and slag, Cem. Concr. Res. 29 (1999) 487–495, https://doi.org/10.1016/S0008-8846(98)00192-6.
[10] J.M. Frederiksen, L. Mejlbro, L.-O. Nilsson, Fick's 2nd Law - Complete Solutions for Chloride Ingress into Concrete - With Focus on Time Dependent Diffusivity and Boundary Condition, (2008).
[11] L.O. Nilsson, J.M. Frederiksen, On uncertainties and inaccuracies in empirical chloride ingress modelling, Eur. J. Environ. Civ. Eng. 15 (2010) 981–990, https://doi.org/10.3166/EJECE.15.981-990.
[12] K.A. Riding, M.D.A. Thomas, K.J. Folliard, Apparent diffusivity model for concrete containing supplementary cementitious materials, ACI Mater. J. 110 (2013) 705–713, https://doi.org/10.14359/51686338.
[13] K. De Weerdt, B. Lothenbach, M.R. Geiker, Comparing chloride ingress from seawater and NaCl solution in Portland cement mortar, Cem. Concr. Res. 115 (2019) 80–89, https://doi.org/10.1016/j.cemconres.2018.09.014.
[14] P. Hemstad, A. Machner, K. De Weerdt, The effect of artificial leaching with HCl on chloride binding in ordinary Portland cement paste, Cem. Concr. Res. 130 (2020), https://doi.org/10.1016/j.cemconres.2020.105976.
[15] A. Machner, P. Hemstad, K. De Weerdt, Towards the understanding of the pH dependency of the chloride binding of Portland cement pastes, Nord. Concr. Res. 58 (2018) 143–162, https://doi.org/10.2478/ncr-2018-0009.
[16] S. Sui, F. Georget, H. Maraghechi, W. Sun, K. Scrivener, Towards a generic approach to durability: factors affecting chloride transport in binary and ternary cementitious materials, Cem. Concr. Res. 124 (2019) 105783, https://doi.org/10.1016/j.cemconres.2019.105783.
[17] ASTM, C1202, Electrical Indication of Concrete's Ability to Resist Chloride Ion Penetration, ASTM International, West Conshohocken, PA, 2012.
[18] NT BUILD 492, Concrete, Mortar and Cement-Based Materials: Chloride Migration Coefficient from Non-Steady-State Migration Experiments, Nordtest, Taastrup, Denmark, 1999.
[19] CSA A23.1, Béton: Constituants et exécution des travaux, Association canadienne de normalisation (CSA), Mississauga, Canada, 2009.
[20] SN EN 13670, Execution of Concrete Structures, Zurich, Switzerland, (2009).
[21] AASHTO TP 95, Standard Method of Test for Surface Resistivity Indication of Concrete's Ability to Resist Chloride Ion Penetration, American Association of State and Highway Transportation, Washington, DC, 2014.
[22] ASTM C1876, Bulk Electrical Resistivity or Bulk Conductivity of Concrete, ASTM International, West Conshohocken, PA, 2019.
[23] J.D. Shane, C.D. Aldea, N.F. Bouxsein, T.O. Mason, H.M. Jennings, S.P. Shah, Microstructural and pore solution changes induced by the rapid chloride permeability test measured by impedance spectroscopy, Concr. Sci. Eng. 1 (1999) 110–119.
[24] A.A. Ramezanianpour, A. Pilvar, M. Mahdikhani, F. Moodi, Practical evaluation of relationship between concrete resistivity, water penetration, rapid chloride penetration and compressive strength, Constr. Build. Mater. 25 (2011) 2472–2479, https://doi.org/10.1016/j.conbuildmat.2010.11.069.
[25] J. Tanesi, A. Ardani, Surface Resistivity Test Evaluation as an Indicator of the Chloride Permeability of Concrete, (2012), https://doi.org/10.1159/000112919.
[26] Y. Dhandapani, T. Sakthivel, M. Santhanam, R. Gettu, R.G. Pillai, Mechanical properties and durability performance of concretes with limestone calcined clay cement (LC3), Cem. Concr. Res. 107 (2018) 136–151, https://doi.org/10.1016/j.cemconres.2018.02.005.
[27] W. Wilson, V. Labattaglia, A. Tagnit-Hamou, L. Sorelli, Will blended-cement systems with similar chloride penetration potentials resist similarly to corrosion, Proc. Sixth Int. Conf. Durab. Concr. Struct. (2018) 587–591.
[28] C. Shi, Another Look at the Rapid Chloride Permeability Test (ASTM C1202 or ASSHTO T277), FHWA Resour. Center, Balt, 2003https://collaboration.fhwa.dot.gov/dot/fhwa/hpc/Lists/aReferences/Attachments/251/RAPCL202RHime.pdf , Accessed date: 22 September 2020.
[29] Y. Dhandapani, M. Santhanam, Assessment of pore structure evolution in the limestone calcined clay cementitious system and its implications for performance, Cem. Concr. Compos. 84 (2017) 36–47, https://doi.org/10.1016/j.cemconcomp.2017.08.012.
[30] G.E. Archie, The electrical resistivity log as an aid in determining some reservoir characteristics, Trans. AIME 146 (1942) 54–62, https://doi.org/10.2118/942054-G.
[31] E.J. Garboczi, Permeability, diffusivity, and microstructural parameters: a critical review, Cem. Concr. Res. 20 (1990) 591–601.
[32] W.J. Weiss, R.P. Spragg, O.B. Isgor, M.T. Ley, T. Van Dam, D.A. Hordijk, M. Luković (Eds.), Toward Performance Specifications for Concrete: Linking Resistivity, RCPT and Diffusion Predictions Using the Formation Factor for Use in Specifications BT - High Tech Concrete: Where Technology and Engineering Meet, Springer International Publishing, Cham, 2018, pp. 2057–2065.
[33] W.J. Weiss, T.J. Barrett, C. Qiao, H. Todak, Toward a specification for transport properties of concrete based on the formation factor of a sealed specimen, Adv. Civ. Eng. Mater. 5 (2016), https://doi.org/10.1520/acem20160004 20160004.
[34] V.J. Azad, A.R. Erbektas, C. Qiao, O.B. Isgor, W.J. Weiss, Relating the formation factor and chloride binding parameters to the apparent chloride diffusion coefficient of concrete, J. Mater. Civ. Eng. 31 (2019), https://doi.org/10.1061/(ASCE)MT.1943-5533.0002615.
[35] M.A.B. Promentilla, T. Sugiyama, T. Hitomi, N. Takeda, Quantification of tortuosity in hardened cement pastes using synchrotron-based X-ray computed microtomography, Cem. Concr. Res. 39 (2009) 548–557, https://doi.org/10.1016/j.cemconres.2009.03.005.
[36] P. Panchmatia, J. Olek, N. Whiting, Electrical conductivity of concrete: the effects of temperature, saturation and air content, Indian Concr. J. 89 (2015) 17–25.
[37] K.Y. Ann, S.I. Hong, Modeling chloride transport in concrete at pore and chloride binding, ACI Mater. J. 115 (2018) 595–604, https://doi.org/10.14359/51702194.
[38] N. Neithalath, J. Jain, Relating rapid chloride transport parameters of concretes to

microstructural features extracted from electrical impedance, Cem. Concr. Res. 40 (2010) 1041–1051, https://doi.org/10.1016/j.cemconres.2010.02.016.
[39] P. Yang, G. Sant, N. Neithalath, A refined, self-consistent Poisson-Nernst-Planck (PNP) model for electrically induced transport of multiple ionic species through concrete, Cem. Concr. Compos. 82 (2017) 80–94, https://doi.org/10.1016/j.cemconcomp.2017.05.015.
[40] Y. Dhandapani, M. Santhanam, Investigation on the microstructure-related characteristics to elucidate performance of composite cement with limestone-calcined clay combination, Cem. Concr. Res. 129 (2020) 105959, https://doi.org/10.1016/j.cemconres.2019.105959.
[41] G.A. Narsilio, R. Li, P. Pivonka, D.W. Smith, Comparative study of methods used to estimate ionic diffusion coefficients using migration tests, Cem. Concr. Res. 37 (2007) 1152–1163, https://doi.org/10.1016/j.cemconres.2007.05.008.
[42] F.P. Glasser, J. Marchand, E. Samson, Durability of concrete - degradation phenomena involving detrimental chemical reactions, Cem. Concr. Res. 38 (2008) 226–246, https://doi.org/10.1016/j.cemconres.2007.09.015.
[43] T. Sanchez, P. Henocq, O. Millet, A. Aït-Mokhtar, Coupling PhreeqC with electro-diffusion tests for an accurate determination of the diffusion properties on cementitious materials, J. Electroanal. Chem. 858 (2020), https://doi.org/10.1016/j.jelechem.2019.113791 113791.
[44] M. Zalzale, P.J. McDonald, Lattice Boltzmann simulations of the permeability and capillary adsorption of cement model microstructures, Cem. Concr. Res. 42 (2012) 1601–1610, https://doi.org/10.1016/j.cemconres.2012.09.003.
[45] NT BUILD 355, Concrete, Mortar and Cement-based Materials: Chloride Diffuson Coefficient from Migration Cell Experiment, Nordtest, Taastrup, Denmark, 1997.
[46] C. Andrade, Calculation of chloride diffusion coefficients in concrete from ionic migration measurements, Cem. Concr. Res. 23 (1993) 724–742, https://doi.org/10.1016/0008-8846(94)90067-1.
[47] P.F. McGrath, R.D. Hooton, Influence of voltage on chloride diffusion coefficients from chloride migration tests, Cem. Concr. Res. 26 (1996) 1239–1244, https://doi.org/10.1016/0008-8846(96)00094-4.
[48] O. Truc, J.P. Ollivier, M. Carcassès, New way for determining the chloride diffusion coefficient in concrete from steady state migration test, Cem. Concr. Res. 30 (2000) 217–226, https://doi.org/10.1016/S0008-8846(99)00232-X.
[49] E. Samson, J. Marchand, K.A. Snyder, Calculation of ionic diffusion coefficients on the basis of migration test results, Mater. Struct. Constr. 36 (2003) 156–165, https://doi.org/10.1617/14002.
[50] C. Andrade, M.A. Sanjuán, Experimental procedure for the calculation of chloride diffusion coefficients in concrete from migration tests, Adv. Cem. Res. 6 (1994) 127–134, https://doi.org/10.1680/adcr.1994.6.23.127.
[51] P. Henocq, E. Samson, J. Marchand, Portlandite content and ionic transport properties of hydrated C 3S pastes, Cem. Concr. Res. 42 (2012) 321–326, https://doi.org/10.1016/j.cemconres.2011.10.001.
[52] J. Marchand, E. Samson, Y. Maltais, Method for Modeling the Transport of Ions in Hydrated Cement Systems, US 6,959,270, (2005).
[53] S. Sui, W. Wilson, F. Georget, H. Maraghechi, H. Kazemi-Kamyab, W. Sun, K. Scrivener, Quantification methods for chloride binding in Portland cement and limestone systems, Cem. Concr. Res. 125 (2019), https://doi.org/10.1016/j.cemconres.2019.105864 105864.
[54] F. Georget, W. Wilson, K. Scrivener, edxia, microstructure characterisation from quantified SEM-EDS hypermaps, Cem. Concr. Res. (2020) (In Revision).
[55] J.O. Bockris, A.K.N. Reddy, Modern Electrochemistry, (1970), https://doi.org/10.1007/978-1-4615-7467-5.
[56] C. Gallé, Effect of drying on cement-based materials pore structure as identified by mercury intrusion porosimetry - a comparative study between oven-, vacuum-, and freeze-drying, Cem. Concr. Res. 31 (2001) 1467–1477, https://doi.org/10.1016/S0008-8846(01)00594-4.
[57] R.S. Barneyback, S. Diamond, Expression and analysis of pore fluids from hardened cement pastes and mortars, Cem. Concr. Res. 11 (1981) 279–285, https://doi.org/10.1016/0008-8846(81)90069-7.
[58] S.Y. Hong, F.P. Glasser, Alkali binding in cement pastes: part I. The C-S-H phase, Cem. Concr. Res. 29 (1999) 1893–1903, https://doi.org/10.1016/S0008-8846(99)00187-8.
[59] Y. Elakneswaran, A. Iwasa, T. Nawa, T. Sato, K. Kurumisawa, Ion-cement hydrate interactions govern multi-ionic transport model for cementitious materials, Cem. Concr. Res. 40 (2010) 1756–1765, https://doi.org/10.1016/j.cemconres.2010.08.019.
[60] O.B. Isgor, W.J. Weiss, A nearly self-sufficient framework for modelling reactive-transport processes in concrete, Mater. Struct. Constr. 52 (2019), https://doi.org/10.1617/s11527-018-1305-x.
[61] M.R. Nokken, R.D. Hooton, Using pore parameters to estimate permeability or conductivity of concrete, Mater. Struct. 41 (2007) 1–16, https://doi.org/10.1617/s11527-006-9212-y.